

Fairness Properties of Face Recognition and Obfuscation Systems

Harrison Rosenberg

University of Wisconsin–Madison
hrosenberg@ece.wisc.edu

Kassem Fawaz

University of Wisconsin – Madison
kfawaz@wisc.edu

Brian Tang

University of Wisconsin–Madison
bjtang2@wisc.edu

Somesh Jha

University of Wisconsin – Madison
jha@cs.wisc.edu

Abstract

The proliferation of automated facial recognition in various commercial and government sectors has caused significant privacy concerns for individuals. A recent and popular approach to address these privacy concerns is to employ evasion attacks against the metric embedding networks powering facial recognition systems. Face obfuscation systems generate imperceptible perturbations, when added to an image, cause the facial recognition system to misidentify the user. The key to these approaches is the generation of perturbations using a pre-trained metric embedding network followed by their application to an online system, whose model might be proprietary. This dependence of face obfuscation on metric embedding networks, which are known to be unfair in the context of facial recognition, surfaces the question of demographic fairness – *are there demographic disparities in the performance of face obfuscation systems?* To address this question, we perform an analytical and empirical exploration of the performance of recent face obfuscation systems that rely on deep embedding networks. We find that metric embedding networks are demographically aware; they cluster faces in the embedding space based on their demographic attributes. We observe that this effect carries through to the face obfuscation systems: faces belonging to minority groups incur reduced utility compared to those from majority groups. For example, the disparity in average obfuscation success rate on the online Face++ API can reach up to 20 percentage points. Further, for some demographic groups, the average perturbation size increases by up to 17% when choosing a target identity belonging to a different demographic group versus the same demographic group. Finally, we present a simple analytical model to provide insights into these phenomena.

1 Introduction

Automated facial recognition has proliferated in various commercial and government sectors. Facial recognition systems can identify users on social media, search for missing persons, aid law enforcement and surveillance, and verify identities of individuals [1, 2]. The widespread adoption of facial recognition systems has been swift with the emergence of metric embedding networks such as FaceNet [3] and ArcFace [4] as well as the abundance of labeled face data [5, 6].

Recent media coverage of data breaches, violation of privacy laws, and the adoption of face recognition by law enforcement entities have shed light on the significant security and privacy implications of face recognition systems. To mitigate the growing privacy concerns, face obfuscation systems have been proposed to hide the identity of users. Several of these systems, such as Face-off [7], LowKey [8], and Foggysight [9], leverage the properties of evasion attacks against machine learning models [10–12]. In the context of facial recognition, the evasion attack runs against the underlying metric embedding network. By introducing small and imperceptible perturbations to their face, a user can evade identification by a facial recognition system.

Such systems are attractive for end-user applications: the perturbations are often acceptable to the user; several features of social media applications, such as filters, do not suffer; and the obfuscation mechanism runs locally, without access to target facial recognition systems. The last feature is enabled by the transferability property of evasion attacks, whereby perturbations are effective against different models running the same task.

These facial obfuscation systems, however, suffer major shortcomings. One has been identified just recently: the face recognition system can adapt and use perturbed faces to improve its performance [13] – perturbed faces can be re-identified in the future. In this work, we uncover another shortcoming of such systems: *there are demographic disparities in the performance of face obfuscation systems that are based on evasion attacks*. This disparity leads to the following research questions:

- Are the metric embedding networks underlying face obfuscation systems aware of the demographic attributes of faces?
- How does the behavior of face obfuscation systems depend on the demographic attributes of faces?
- Can the dependencies on demographic group of face recognition and obfuscation models be explained via an analytical model?

This paper presents a systematic characterization of the demographic disparities of face obfuscation systems and their underlying metric embedding networks¹. Previous research has studied the fairness and robustness properties of face recognition [14, 15] in the classification setting. However, we study the fairness properties of facial recognition and obfuscation in the context of the metric embedding networks – the real-world setting for such systems. Our empirical and analytical characterization yields the following insights about the fairness implications of face recognition and obfuscation.

Are the metric embedding networks underlying face obfuscation systems aware of the demographic attributes of faces? As face obfuscation systems directly rely on the underlying metric embedding network, it is important to study if these models are aware of the demographic attributes of faces. We perform our experiments on FaceNet [3] and two well-established benchmark datasets in facial recognition: Labeled Faces in the Wild (LFW) [5] and VGGFace2 [6]. First, we characterize the accuracy of modern facial recognition systems when conditioned on demographic attributes. We observe that the underlying models distinguish individuals of different demographic attributes more effectively than those of the same attribute. For example, these models underperform for female faces compared to male faces.

Second, using estimates of local Lipschitz constants [16], we find facial recognition systems to be less stable when trained on imbalanced datasets, especially around samples from minority demographic groups. This instability contributes to performance degradation for minority groups. Third, we observe that these models learn demographic attributes as concepts without having explicit access to them during the training. Using TCAV scores [17], we find that FaceNet uses learned concepts such as skin tone and sex-correlated facial features in its predictions. Unsurprisingly, when we visualize the face in the embedding space using t-SNE [18], we find faces belonging to the same skin tone or sex tend to be more tightly clustered. More details are in section 5.

How does the behavior of face obfuscation systems depend on the demographic attributes of faces? We analyze two recent face obfuscation systems: Face-Off [7], a proxy for targeted obfuscation, and LowKey [8], a proxy for untargeted obfuscation. At a first glance, the instability of facial recognition systems around samples from minority groups can benefit the application of face obfuscation; this instability is supposed to make evasion attacks easier to construct. We observe that to be the case for targeted attacks

¹We plan to make our codebase and results publicly available.

in the white-box setting; faces from minority groups enjoy smaller perturbation sizes. This advantage, however, disappears when analyzing the obfuscation success rate in black-box settings, such as the Face++ face recognition API. There, the perturbed faces from majority groups have a higher obfuscation success rate. We attribute this discrepancy to the size of the perturbations [7, 19] as faces from majority groups result in larger and more robust perturbations. Recall that the real-world application of face obfuscation systems involves generating the perturbed face using a surrogate model with the intent that it transfers to a black-box model. As such, minority users of such systems suffer in terms of reduced utility from face obfuscation.

Delving deeper into the behavior of face obfuscation with respect to source and target demographic groups, we find such systems to retain the demographic attribute of the face. We find that untargeted attacks almost always result in perturbed faces that match the demographic attributes of the source faces. Further, we find the embeddings of the natural faces to completely overlap those of perturbed faces (in the untargeted case) when visualized using t-SNE. The user of such systems is more successful at changing their identity to one within their demographic group. Otherwise, they will incur larger, more visible perturbations to their faces if they choose a target identity from a different demographic group. More details are in section 6.

Can the dependencies on demographic group of face recognition and obfuscation models be explained via an analytical model?

We devise an analytical model, based on a mixture of Gaussian distributions and Principal Component Analysis (PCA), to formalize the behavior of face recognition and obfuscation when conditioning on the demographic group. Our model reveals two insights that help formalize our empirical observations. First, we find that the representation ability of the embedding function depends on the balance in sampling from different groups; a group with higher contribution to the training data results in more representative embedding. Second, when embeddings are clustered, a bounded adversarial perturbation belongs to the same group as the input. This model, while simple, is a powerful tool to analyze the demographic disparities in face recognition and obfuscation. More details are in section 4.

2 Background

To understand the context of face obfuscation systems, it is necessary to discuss some of the notation, background, and tools used with neural networks and face recognition. We use the following notation throughout this paper.

2.1 Notation and Terminology

We consider the setting in which there exists an input space $\mathcal{X} \subseteq \mathbb{R}^d$ and a discrete label set \mathcal{Y} . A subset of examples, also referred to as a dataset, is denoted as $S \subseteq \mathcal{X} \times \mathcal{Y}$. Sometimes we abuse notation and let S contain only unlabeled examples $\{\mathbf{x}_1, \mathbf{x}_2, \dots\}$. A sample \mathbf{x} is a d -dimensional real-valued vector. Often in our setting, \mathbf{x} refers to a cropped face, d to the number of pixels in the cropped face multiplied by three (referring to the RGB color channels), and \mathcal{Y} to the set of identities.

Throughout this paper, scalars are denoted by lowercase standard-typeface letters, vectors are denoted by boldface lowercase letters, sets are denoted by capital letters and matrices are denoted by boldface capital letters. Given a vector \mathbf{z} , z_j denotes the j^{th} entry in vector \mathbf{z} . Given a matrix \mathbf{A} , A_{ij} denotes the entry of matrix \mathbf{A} at row i , column j . If a matrix is itself indexed by a subscript, such as \mathbf{A}_b , the example at row i , column j is denoted $(\mathbf{A}_b)_{ij}$. Probability distributions are denoted with calligraphic capital letters. We will use \mathcal{D} to represent the distribution from which examples in training data S are drawn. $\mathbb{1}$ denotes the indicator function. Let z be a Boolean expression. $\mathbb{1}[z]$ evaluates to 1 if z is true, otherwise $\mathbb{1}[z]$ evaluates to 0. A metric is denoted by $\rho : \mathcal{X} \times \mathcal{X} \rightarrow \mathbb{R}_+$. Sometimes we abuse notation such that metric ρ is given only one argument. When this is the case, the second argument to the metric ρ is implicitly a size conforming

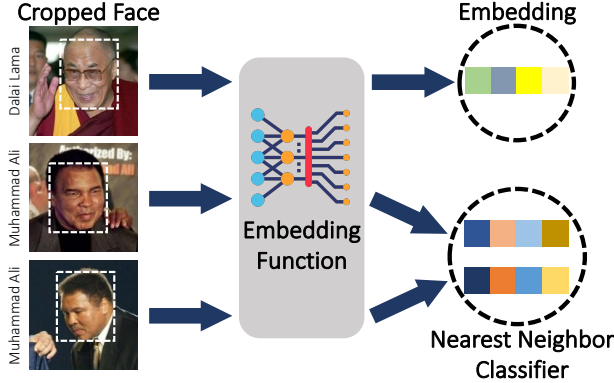


Figure 1: For well-trained embedding functions, embeddings of images belonging to the same identity will have smaller pairwise distances than the pairwise distances between embeddings of different identities. Note that a *metric embedding network* refers to an “embedding function” with a DNN architecture.

zero vector.

The terminology with respect to population demographics used in this paper follows that of Buolamwini and Gebru [14] and Nanda et al. [15], two leading works on facial recognition fairness. In the dataset annotations, there are only two sexes, hence we use “male” and “female.” As for ethnicity, previous literature utilizes terms such as “White,” “Black,” “Asian,” and “Indian” within their attribute annotations [20]. We find it more accurate to refer to these demographic labels as “race.” For consistency, we use the same demographic attribute labels in the VGGFace2 dataset in our facial recognition and face obfuscation performance evaluations.

2.2 Face Recognition System

A facial recognition system decomposes into two sequential components: a *metric embedding network* and a *nearest neighbors classifier*. The metric embedding network, denoted by $f_k : \mathbb{R}^d \rightarrow \mathbb{R}^k$, is a neural network which takes an RGB face image \mathbf{x} as input, and returns a k dimensional embedding. We sometimes omit the subscript k when referring to a generic embedding function. The goal of a metric embedding network is to map high dimensional images into an embedding space such that images belonging to the same identity have lower pairwise distance in the embedding space. Likewise, images belonging to different identities are intended to have high pairwise distance in the embedding space. To achieve such behavior, metric embedding networks are trained with contrastive loss functions, such as triplet loss [3]. The functionality of a face recognition system is depicted in fig. 1.

Upon obtaining an embedding output by a metric embedding network, one can perform tasks such as clustering, matching, or classification. This nearest neighbors classifier H is the second component in the facial recognition pipeline. Given an input image \mathbf{x}' , the nearest neighbor classifier H yields the identity y of the nearest embedding to $f(\mathbf{x}')$, where $y \in \mathcal{Y}$. The facial recognition system uses a distance metric such as ℓ_2 norm or cosine similarity to determine the distance between embeddings. Given a training set S , an unlabeled example \mathbf{x} , an embedding function f , and a metric ρ , the nearest neighbor classifier is defined to be:

$$H(\mathbf{x}) \triangleq \arg \min_{y' | (\mathbf{x}', y') \in S} \rho(f(\mathbf{x}'), f(\mathbf{x})) \quad (1)$$

Note that eq. (1) represents the entire facial recognition system upon which our experiments are based.

2.3 Principal Component Analysis

The Principal Component Analysis (PCA) forms the backbone for our analytical model (section 4). PCA is a well-known linear dimensionality reduction algorithm [21]. By finding a new basis for the dataset, PCA can uncover hidden or otherwise non-obvious patterns therein. In particular, PCA constructs an ordered orthonormal basis for a given mean-centered dataset. The orthonormal basis vectors are arranged in decreasing order of their variance contribution to the original dataset. PCA may be familiar to readers in its relationship to the Singular Value Decomposition (SVD). The square of the i^{th} singular value represents the variance contributed by the i^{th} principal component. Though PCA refers to a linear operation, we will see in section 4 how to utilize PCA to explore the concept of embeddings and metric embedding networks in general.

2.4 t-SNE

The t-Distributed Stochastic Neighbor Embedding (t-SNE) [18] is another dimensionality reduction technique which is useful in visualizing high dimensional embedding spaces. t-SNE is often used in visualizing image datasets or deep neural network embeddings in two or three dimensions. It is a variation on Stochastic Neighbor Embeddings [22] which avoids crowding data points and can capture the implicit structure of data. In this paper, we use t-SNE to visualize the embedding of faces as in fig. 3; such plots aid our discussion of the embedding space geometry.

2.5 TCAV

TCAV [17] is a tool used to evaluate the interpretability of a deep neural network. Using user-specified high-level concepts, such as patterns or colors, decision boundaries are created by training linear classifiers on a neural network’s activations for a given concept’s examples. Concept Activation Vectors (CAVs) are extracted from the vector orthogonal to this decision boundary, and a statistical significance test is performed on these CAVs and the model’s gradients. Though TCAV has been traditionally used to map learned concepts in classification networks, we extend its functionality to metric embedding networks so that we may better understand the contributing factors in a deep neural network’s predictions. In section 5.3, we explore which layers the network uses to distinguish the high-level concepts of race and sex in the construction of an embedding.

2.6 Relevant Fairness Definitions

There is no single definition of fairness, mathematical or otherwise [23]. Hence, we study several quantities which have an intuitive connection to both facial recognition and face obfuscation systems. These quantities include a comparison, by demographic, of the success rates of face obfuscation systems as measured by perturbation success rate. When these success rates are equal, they satisfy the fairness constraint known as statistical parity [24]. We also compare, by demographic, the strength of such perturbations necessary to yield a successful face obfuscation. For targeted evasion attacks, we study the strength of such perturbations in both the inter-demographic group and intra-demographic group settings. We also study how likely untargeted perturbations are to change the perceived demographic of an image.

2.7 Adversarial Machine Learning

Goodfellow et al. [10] discovered an interesting property of deep neural networks: they are vulnerable to adversarial examples. Small structured perturbations, imperceptible to the human eye, may cause the network to misclassify a given input sample. This branch of machine learning research resulted in the formulation

of many attack algorithms, the most common of which are evasion attacks, including Fast Gradient Sign Method (FGSM) [11], Projected Gradient Descent (PGD) [11], and Carlini-Wagner (CW) [12] attacks. The bulk of study in adversarial machine learning focuses on attacks that algorithmically generate ℓ_p norm-bounded perturbations by performing a noisy gradient-based optimization procedure. We further discuss adversarial machine learning in the context of facial recognition in the next section.

3 Face Obfuscation

Researchers have demonstrated that systems which adversarially perturb inputs to facial recognition systems can provide privacy benefits to users. In this section, we present the notation and discuss the work relevant to such face obfuscation systems.

3.1 Threat Model

In the face obfuscation setting, an end user considers the machine learning provider to be the main threat. They wish to apply (imperceptible) perturbations to their faces, prior to uploading them, so that they are misclassified. Such protection might be beneficial in the event of social media data leaks [25], preventing cyber-stalking [26], protecting data from web scrapers, hiding online activity from big government entities [27, 28], and more.

State-of-the-art designs for face obfuscation systems leverage evasion attacks, such as those described in section 2.7. Unlike other attacks, evasion attacks assume the user is not able to poison the face recognition system. An important characteristic of adversarial examples, especially for vision tasks such as facial recognition, is their ability to transfer across models. This property allows users to generate adversarial examples without requiring access to an online face recognition API and without directly querying said model. Instead, face obfuscation systems leverage this properties by querying surrogate models to generate the perturbed faces. In a *white-box* setting, examples are generated with the intention of attacking the surrogate model. In the *black-box* setting, examples are generated on the surrogate model and applied to a black-box model, by leveraging the transferability property.

3.2 Face Obfuscation Systems

The earliest work in this vein of face obfuscation research explores physical adversarial examples. For example, Sharif et al. [29] present physically realizable glasses that allow a user to impersonate a target individual or evade face detection systems. Recently, there has been a shift in focus towards preserving user privacy online from malicious web scrappers, data breaches, and curious service providers. Thus, researchers have focused more on digital face obfuscation systems, which are more suited for social media and online applications. Examples of such systems include FAWKES [30], Face-Off [7], Low-Key [8], and FoggySight [9]. With the exception of FAWKES, which leverages data poisoning attacks, these face obfuscation systems utilize evasion attacks with an attempt to hide the user’s identity. These systems are the main focus of this paper.

We now describe these face obfuscation systems more formally. Let Δ denote an evasion attack function (e.g. PGD, CW), and let δ denote a generic perturbation output by the evasion attack function, i.e. $\Delta(x)$. A face obfuscation system feeds $x + \delta$ into the facial recognition system. Note that perturbation function Δ may include dependence on the metric embedding network, the underlying dataset, or some other surrogate model. Throughout this work, we explore how these face obfuscation systems fare for each demographic under a variety of adversarial attack algorithms.

3.3 Evasion Attacks on Facial Recognition

Evasion attacks may be divided into targeted and untargeted varieties. To define the two attacks, we first describe the embedding centroid. Given a dataset S , denote by $c_{f,y}$ the embedding centroid for identity y as computed on embedding function f is:

$$c_{f,y} \triangleq \frac{1}{|\{(x', y') \in S \mid y' = y\}|} \sum_{(x', y') \in S} f(x') \cdot \mathbb{1}[y' = y] \quad (2)$$

Untargeted Attacks: Recall from section 2.1 that a metric ρ given only one explicit argument is assumed to have a size-conforming zero vector as its second argument. Given a metric embedding network $f : \mathcal{X} \rightarrow \mathcal{Y}$ unlabeled example x , and metrics ρ_1, ρ_2 an *untargeted attack* may be formulated as follows:

$$\begin{aligned} & \min_{\delta \mid x + \delta \in \mathcal{X}} \rho_1(\delta) \\ \text{s.t. } & \arg \min_{y' \in \mathcal{Y}} \rho_2(c_{f,y'}, f(x)) \neq \arg \min_{y' \in \mathcal{Y}} \rho_2(c_{f,y'}, f(x + \delta)) \end{aligned} \quad (3)$$

The problem with the formulation above is that the constraint is non-convex. To make the attack implementable in practice, the constraints must be relaxed. For a labeled example (x, y) , the optimization objective which yields an untargeted perturbation can be written as:

$$\arg \max_{\delta \mid x + \delta \in \mathcal{X}} \rho_2(f(x + \delta), c_{f,y}) \quad \text{s.t.} \quad \rho_1(\delta) \leq \epsilon \quad (4)$$

In this paper, we use the LowKey attack [8] to instantiate eq. (4). In this case, PGD is used to solve the optimization problem, ρ_1 is the Learned Perceptual Image Patch Similarity (LPIPS) metric [31], and ρ_2 is the distance between the original face and perturbed face in the embedding space. Note that the latter distance is averaged through an ensemble of models and after applying Gaussian smoothing.

Targeted Attacks: Given a target label y' , metric embedding network $f : \mathcal{X} \rightarrow \mathcal{Y}$ unlabeled example x , and metrics ρ_1, ρ_2 a *targeted attack* may be formulated as follows:

$$\min_{\delta \mid x + \delta \in \mathcal{X}} \rho_1(\delta) \quad \text{s.t.} \quad y' = \arg \min_{y \in \mathcal{Y}} \rho_2(c_{f,y}, f(x + \delta)) \quad (5)$$

Similar to the untargeted case, attacks on facial recognition systems relax the above constraints to arrive at a convex optimization formulation. Here, we state one such relaxation from Face-Off [7], which we use in the rest of this paper. First, we define the multi-class hinge loss. The multi-class hinge loss enables a convex relaxation of the constraints in the targeted attack eq. (5). Given a perturbed example $x + \delta$, target label y' , and positive real number κ , the multi-class hinge loss is denoted by $G_\kappa(x + \delta, y')$ where:

$$\begin{aligned} G_\kappa(x + \delta, y') \triangleq & \max \left\{ 0, \kappa + \rho_2(x + \delta, c_{f,y'}) \right. \\ & \left. - \max_{y \neq y'} \rho_2(x + \delta, c_{f,y}) \right\} \end{aligned} \quad (6)$$

For a labeled example (x, y) , and target label $y' \neq y$, the CW attack can minimize the following optimization objective:

$$\arg \min_{\delta \mid x + \delta \in \mathcal{X}} \rho_1(\delta) \quad \text{s.t.} \quad \rho_1(\delta) \leq \epsilon \quad \text{and} \quad G_\kappa(x + \delta, y') \leq 0 \quad (7)$$

4 Analytical Model

To understand the fairness issues associated with facial recognition and obfuscation, we present a tractable, simplified model on synthetic data. This model is inspired by the hierarchical nature of popular facial recognition datasets. The synthetic data consists of examples drawn from a parametrized hierarchical Gaussian mixture we define in section 4.1. We use a k -component PCA as an embedding function – a PCA embedding function which only utilizes projections onto the leading k principal components to perform its dimensionality reduction – because it is useful for our analysis. Such analysis is common in the space of machine learning. Though all samples drawn from our simplified model are vectors, we use the terms *identity* and *image* to draw parallels between the hierarchical nature of our probabilistic model and the hierarchical structure of existing facial recognition datasets.

4.1 Setup

Similar to empirical datasets, we analyze our synthetic dataset by conditioning on a simulated demographic group. Within the dataset, there are two mutually exclusive population groups: group a and group b. We sometimes use a placeholder g to represent a group $g \in \{a, b\}$. The mean vector for population groups a and b are denoted by $\mu_a \in \mathbb{R}^d$ and $\mu_b \in \mathbb{R}^d$, respectively. Moreover, $\mu_a = -\mu_b$, $\|\mu_a\|_2 = 1$, and $\|\mu_b\|_2 = 1$.

The i^{th} identity in group g is denoted by $\nu_{g,i} \in \mathbb{R}^d$. The j^{th} image representing identity $\nu_{g,i}$ is denoted by $x_{g,i,j} \in \mathbb{R}^d$. $\Sigma_a \in \mathbb{R}^{d \times d}$ and $\Sigma_b \in \mathbb{R}^{d \times d}$ are diagonal covariance matrices. Furthermore, $\Sigma_a = \gamma \Sigma_b$ where γ is a positive, real-valued scalar. An identity $\nu_{g,i}$ is drawn from the identity distribution $\mathcal{N}(\mu_g, \Sigma_g)$. The identity distribution may be thought of as a hyperprior on images. An image $x_{g,i,j}$ is drawn from $\mathcal{N}(\nu_{g,i}, \beta \mathbf{I})$ where β is a positive, real-valued number. Moreover, for each identity $\nu_{g,i}$, exactly m images are drawn from $\mathcal{N}(\nu_{g,i}, \beta \mathbf{I})$. Lastly, we denote by \mathcal{D}_g the distribution of images in group g .

The synthetic data distribution is a linear combination of image distributions for group a (\mathcal{D}_a) and group b (\mathcal{D}_b). Let $\alpha_a \in [0, 1]$ denote the proportion of examples drawn from group a and let $\alpha_b \in [0, 1]$ denote the proportion of examples drawn from b. Since the population groups are mutually exclusive, we know $\alpha_a + \alpha_b = 1$. The synthetic data distribution, we denote by \mathcal{D} is a linear combination, that is $\mathcal{D} = \alpha_a \mathcal{D}_a + \alpha_b \mathcal{D}_b$. We denote by S a sampling of images drawn from \mathcal{D} .

4.2 The Ideal Embedding Function

In the context of machine learning, an ideal embedding function $f_k : \mathbb{R}^d \rightarrow \mathbb{R}^k$ is one which preserves distances within a dataset. While this property is important for facial recognition and obfuscation, it is not the only consequential property of embedding functions. In the context of fair facial recognition, we concern ourselves with how well the embedding represents a particular group from the lens of that group. For k component PCA, we introduce a quantity, called the relative projection distance, which captures this concept.

Definition 4.2.1. Let S be a sample of images drawn from the overall synthetic distribution \mathcal{D} . The relative projection distance of a point \mathbf{x} , a member of group g , with respect to the leading k principal components of a dataset S is denoted by $\rho_{\text{rp},S,g,k} : \mathcal{X} \rightarrow \mathbb{R}^+$. More precisely, the quantity is defined as:

$$\rho_{\text{rp},S,g,k}(\mathbf{x}) \triangleq \frac{\left\| \left(\mathbf{x} - \sum_{i=1}^k \left\{ \frac{\mathbf{q}_i^\top \mathbf{x}}{\|\mathbf{q}_i\|_2 \|\mathbf{x}\|_2} \mathbf{q}_i \right\} \right) \right\|_2}{\sum_{j=1}^d (\Sigma_g)_{jj}}, \quad (8)$$

where the eigen-decomposition of the covariance of overall synthetic data distribution \mathcal{D} is $\Sigma = \mathbf{Q} \Lambda \mathbf{Q}^\top$. Furthermore, \mathbf{Q} may be decomposed as $\mathbf{Q} = [\mathbf{q}_1, \dots, \mathbf{q}_d]^\top$.

Let us explain the reasoning behind this formulation of the relative projection distance. The numerator computes the norm of the portion of sample \mathbf{x} which is orthogonal to the subspace spanned by the first k principal components of sample S drawn from \mathcal{D} . This portion of \mathbf{x} is also known as an error vector. The denominator represents a group specific normalization factor. This normalization factor represents the total variance within the identity vectors $\{\nu_{g,1}, \nu_{g,2}, \dots, \}$ of group g . It is this normalization factor which allows us to show how error can be measured through the lens of each group. In summary, the relative projection distance captures the error induced by the embedding function, as measured through the lens of only population group g .

4.3 Instantiating the Embedding Function

Let us now instantiate our synthetic distribution with a k -component PCA as the embedding function f_k . Utilization of this embedding function enables us to show how relative projection distance may vary greatly between demographic groups a and b . Figure 2 depicts how the distribution of relative projection distances induced by f_k may be either equal or disparate when conditioning by population group. For a demographic group, the distribution of relative projection distance depends on how much a population group contributes to the covariance Σ of the overall data distribution \mathcal{D} . The contribution to covariance is measured by the *covariance contribution*. For our synthetic data distribution \mathcal{D} , we compute the covariance contribution from population group g as:

$$\left(\beta + \sum_{i=1}^k (\Sigma_g)_{ii} \right), \quad (9)$$

where k is the number of principal components used in the PCA embedding and Σ_g is the covariance matrix for the group g identity distribution.

From our understanding of the synthetic data distribution developed by decomposition of Σ detailed in appendix A.2, we now put forth a proposition regarding the distribution of relative projection distance amongst examples in each group.

Proposition 4.3.1. *For a population group g , as the covariance contribution (defined in eq. (9)) increases, the relative projection distance (defined in eq. (8)) decreases.*

Note that increases in covariance contribution may come from increasing the number of samples in population group g or by increasing the magnitude of covariance Σ_g .

Upon examining the figs. 2a and 2b, proposition 4.3.1 holds true: In both subfigures, there are 2500 identities per group, making $\alpha_a = \alpha_b = 0.5$. Further, there are $m = 50$ images sampled per identity. In fig. 2b, both groups have identical covariance matrices, but in fig. 2a, $\frac{1}{10000}\Sigma_a = \Sigma_b$.

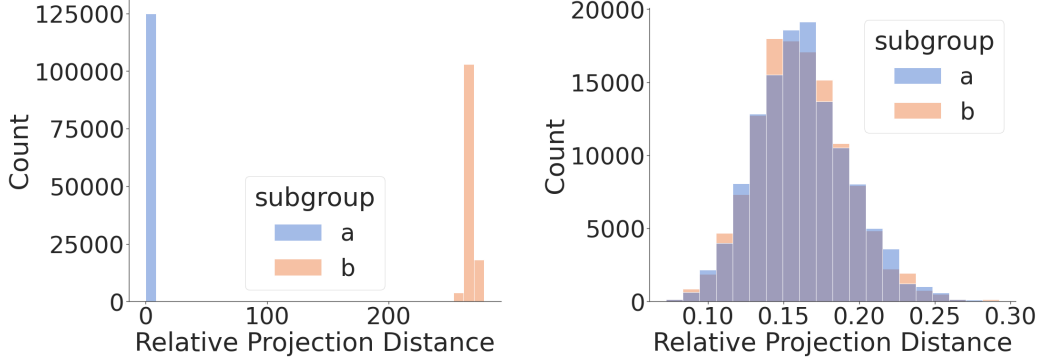
These plots follow the intuition of our proposition exactly: In fig. 2b, the covariance contributions from each group are equal, hence the distribution of relative projection distance is approximately equal for both groups. In fig. 2a, group b has a much smaller covariance contribution than does group a , hence the distribution of relative projection distance for examples within group b is shifted right.

4.4 Connection to Face Obfuscation

To connect our theory to face obfuscation, we discuss the construction of evasion attacks in our analytical model. Denote by $p_{\mathcal{Q}}$ the probability density function for probability distribution \mathcal{Q} . Given an example \mathbf{x} , define the maximum likelihood estimator $\psi(\mathbf{x}) = \arg \max_{g \in \{a,b\}} p_{\mathcal{D}_g}(\mathbf{x})$.

Given an example image \mathbf{x} in group g , we study how difficult it is to construct a perturbation δ such that $\psi(\mathbf{x} + \delta) \neq g$. The synthetic data distribution described in this section is a natural medium with which to quantify the necessary strength of such a perturbation δ :

Let $f : \mathbb{R}^d \rightarrow \mathbb{R}$ be a PCA embedding function. Consider a sample \mathbf{x} drawn from the overall synthetic data distribution \mathcal{D} and without loss of generality assume this \mathbf{x} is a member of group a . Assume $\gamma \leq$



(a) Relative projection distance is plotted for groups a and b with imbalanced covariance contributions.

(b) Relative projection distance is plotted for groups a and b with balanced covariance contributions.

Figure 2: Relative projection distance is plotted for both balanced and imbalanced population groups.

1, $p_{\mathcal{D}_a}[\mu_a] > p_{\mathcal{D}_b}[\mu_a]$, and $p_{\mathcal{D}_b}[\mu_b] > p_{\mathcal{D}_a}[\mu_b]$. Given an adversarial perturbation δ , we assume that perturbation δ is norm-bounded and in the direction $\frac{(\mu_b - x)}{\|\mu_b - x\|_2}$ as it is known to be an adversarial direction. That is, we assume $\|\delta\|_2 \leq \epsilon$ where ϵ is a non-negative real number.

To capture how strong this perturbation δ can be $\psi(x + \delta)$ remains a, we quantify the values of ϵ for which the following optimization problem is guaranteed to be infeasible. If the optimization problem is infeasible then it is guaranteed that $\psi(x + \delta) = a$:

$$\begin{aligned}
 & \min_{\delta: \|\delta\|_2 \leq \epsilon} \|\delta\|_2 \\
 & \text{s.t.} \quad \mathbb{P}_{f(x) \sim \mathcal{D}_b} [f(x + \delta)] > \mathbb{P}_{x \sim \mathcal{D}_a} [f(x + \delta)] \\
 & \quad \delta = \eta \cdot \frac{(\mu_b - x)}{\|\mu_b - x\|_2} \text{ where } \eta \in \mathbb{R}
 \end{aligned} \tag{10}$$

For notational compactness, we denote:

$$a = f(x) \text{ and } b = f\left(\frac{(\mu_b - x)}{\|\mu_b - x\|_2}\right).$$

This optimization objective in eq. (10) guaranteed to be infeasible when:

$$\epsilon < \max \left\{ 0, \frac{2b(\gamma - 1) \sqrt{\frac{a^2 \gamma}{b^2 (\gamma - 1)^2} + a\gamma + a + f(\mu_b)(1 - \gamma)}}{b(\gamma - 1)} \right\} \tag{11}$$

This result is further detailed in appendix A.3.

Therefore we conclude that $\psi(x + \delta) = a$ when inequality (4.4) holds. Furthermore, note that the bound in inequality (11) is not tight, as it becomes more loose as γ approaches 0. Within section 4.4, we notice that for a fixed x for which $\psi(x) = a$, as γ approaches 0, the set of perturbations δ for which $\psi(x + \delta) = a$ increases in size. We conclude that as the variation within group b decreases, the embeddings of samples within group b tend to cluster. Hence, pushing a fixed sample in group a to register as a sample in b becomes more difficult for a face obfuscation system. The relevance of this result will be evident later in sections 5 and 6. The embeddings of faces from minority groups tend to be more concentrated, and we observe that is hard to launch targeted obfuscation towards these groups.

	Male	Female	White	Asian	Black	Indian
ACC	99.11	98.28	99.13	98.04	98.55	95.00
FP	0.43	0.68	0.39	1.04	0.65	0.00
FN	0.46	1.04	0.48	0.92	0.81	5.00
VAL	96.18	85.16	95.94	85.36	92.42	100.00
N	10000	5000	10000	2500	1240	20

Table 1: Same demographic matching performance on LFW. Both accuracy and validation accuracy are lower compared to Table 2. ACC: accuracy, FP: false positive, FN: false negative, VAL: validation accuracy, N : number of pairs.

5 Empirical Characterization of Facial Recognition Systems

Before we study face obfuscation, we empirically characterize the fairness issues associated with the facial recognition systems. In particular, we characterize the dependence of the performance of such systems on the demographic attributes of input faces.

5.1 Face Recognition Setup

Our evaluations focus on two widely-used datasets. For tasks which require multiple images per identity such as training models and running TCAV, we use the VGGFace2 dataset [6]. Though this dataset contains 8631 identities with an average of 362.6 images per identity, it is demographically imbalanced. The demographic split is approximately 60% male and 40% female; and 73% White, 9% Black, 6% Asian, 4% Indian, 4% Middle Eastern, and 4% Latino. During inference time we use the Labeled Faces in the Wild (LFW) dataset [5]. For our evaluation in section 5.2 and section 5.3, we utilize a FaceNet model [3] pre-trained on the VGGFace2 dataset [6], which achieves 99.65% accuracy on the LFW dataset [5]. This Inception ResNet v1 network is trained using triplet loss on $160 \times 160 \times 3$ images and is tuned to output 128-dimensional embeddings. In the next section, we will explore how a neural network trained on an imbalanced dataset performs differently for faces of each demographic group.

5.2 Error Disparity Among Groups

Face recognition models typically optimize for accuracy metrics without explicit consideration for demographic attributes. Still, demographic attributes appear to impact the performance of facial recognition. Tables 1 and 2 demonstrate how training deep neural networks on an imbalanced dataset can result in performance discrepancies. Recall the latter component of facial recognition is essentially a thresholded nearest neighbor classifier; the optimal threshold τ is estimated for the whole training set and evaluated on a validation set. However, the estimated threshold may not be the optimal threshold for each demographic group. When evaluating this model using matching verification, the pairs of identities selected with only the same race or sex (table 1) perform worse when compared to pairs of identities selected without any such demographic restriction (table 2). In groups with fewer samples in the training set, such as female, Asian, and Black identities, these performance gaps are amplified to almost 10 percentage point differences in the validation accuracy. The intra-demographic confusion is higher than inter-demographic confusion, suggesting the model learns to distinguish demographic groups in its predictions.

	Male	Female	White	Asian	Black	Indian
ACC	99.30	98.92	99.15	99.24	99.76	95.00
FP	0.33	0.38	0.35	0.44	0.16	0.00
FN	0.37	0.70	0.50	0.32	0.08	5.00
VAL	96.78	94.36	97.32	94.48	97.42	100.00
N	10000	5000	10000	2500	1240	20

Table 2: Any demographic matching performance on LFW.

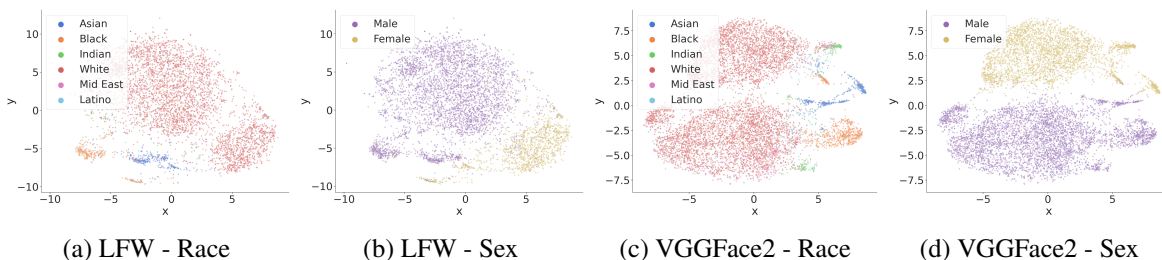


Figure 3: t-SNE [18] of the embedding spaces generated using the LFW [5] and VGGFace2 [6] datasets. Embeddings of identities are colored by race and sex. Distinct clusters exist for each demographic group, some more spread out than others.

5.3 What the Metric Embedding Network Learns

To understand *where* in the metric embedding network architecture these intra-demographic and inter-demographic face determinations are made, we characterize both the embedding space and the intermediate layers of the network. We plot the resulting structure of an embedding of FaceNet using t-SNE [18] in fig. 3. The FaceNet model clusters data points belonging to the same race and sex regardless of whether the data is from training or inference time. This disparity in inter-demographic and intra-demographic embedding distances motivates our exploration of face obfuscation performance in section 6. Interestingly, this clustering appears in the embedding space despite the network never having explicit access to demographic attributes.

We utilize TCAV [17] to investigate whether the intermediate layers of the network learn to distinguish demographic attributes. We retrofit the TCAV framework to fit the metric embedding setting as it is originally defined for classification networks. In particular, we associate each identity with an anchor embedding, corresponding to its embedding centroid. We then use the ℓ_2 distance between the embedding of an input face and its anchor embedding to estimate the gradient from the output layer to the relevant activation layer. For the Facenet metric embedding network, the layers examined include early and intermediate activations towards the end of each inception ResNet block. Our evaluation involves 9 identities for each of the following four races: Asian, Black, Indian, White. In total, we run TCAV on 36 identities, with each identity containing 100 images of a person’s face. Note that on a server equipped with 256 GB of RAM and RTX 2080Ti Nvidia GPUs, it takes several hours to obtain the TCAV score for a single image over multiple layers. As a result, we limited the number of identities we study here.

The concept we study is skin tone. Of the six types of skin tones on the Fitzpatrick scale [32], we select and annotate five types of skin colors ranging from pale white to dark brown. Each skin tone concept contains 75 images cropped from our subset of identities, and each facial region concept contains 250 cropped images. As we conjecture that neural networks are capable of identifying race, we expect at least one layer within the network to explicitly learn this attributes and use them in its output prediction. For the

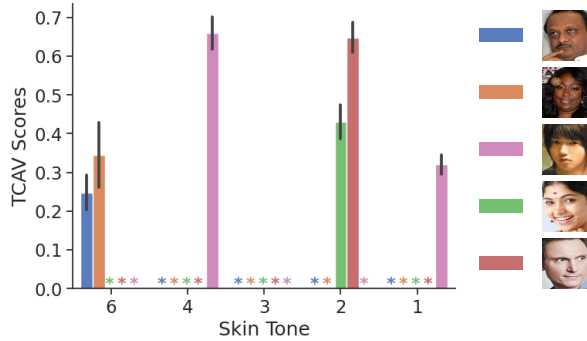


Figure 4: TCAV [17] scores for skin tones. The x-axis represents a range from darker skin (left) to lighter skin (right). TCAV was performed on intermediate layers early in the network. The network learns these concepts for other layers.

FaceNet metric embedding network, the layers examined include early and intermediate activations towards the end of each Inception ResNet block. In fig. 4, we see high utilization of the skin tone concepts by many of the earlier layers in the neural network. Higher TCAV scores indicate concepts which are more significant in the network. The concepts used to differ between identities tend to be correlated with their skin tone.

5.4 Stability Properties of Facial Recognition

Lastly, we investigate the stability of facial recognition networks, in relation to the demographic distribution of their training sets. We do so by examining estimates of the local Lipschitz constants. The margin for these classifiers scales inversely with the Lipschitz constant, making classifiers with high local Lipschitz constants less stable and less generalizable [33–37]. We use the RecurJac [16] and Fast-Lin [38] bound algorithms to estimate the local Lipschitz constant for small neural networks trained on datasets with balanced and imbalanced distributions of demographic groups. Note that the full-fledged DNNs for facial recognition, such as FaceNet, are not amenable to RecurJac and similar estimators. As such, we train two small VGG16 [39] classification networks on balanced and imbalanced datasets of 20 identities with the same number of face images (5 identities per race) from the VGGFace2 dataset. The imbalanced dataset mimics the distribution of the VGGFace2 dataset where White faces have more representation in the number of face images.

Figure 5 shows the distributions of the upper bounds on the estimated local Lipschitz constants for the imbalanced and balanced classifiers; this distribution is plotted for the training set. We observe higher upper bounds in imbalanced versus balanced for each demographic group. Further, identities corresponding to minority demographic groups have higher upper bounds than majority identities. These results are consistent with our earlier observations from the analytical model and empirical observations – the networks generalize less for samples from minority demographic groups. However, the instability ensuing from higher upper bounds on Lipschitz constants does not necessarily imply improved success rate for evasion attacks, as we see later in section 6.

6 Experiments on Face Obfuscation Systems

We wish to understand how biases inherent in both face recognition datasets and metric embedding networks impact the performance of face obfuscation systems. Our objective is to study whether face obfuscation techniques equally benefit different demographic groups. Our experiments focus on answering three questions:

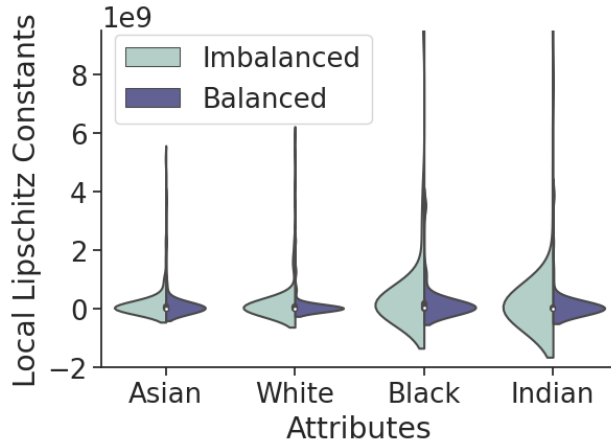


Figure 5: Upper bounds on local Lipschitz constants estimated using Fast-Lin and RecurJac. Models trained on imbalanced demographic distributions suffer from higher instability. The maximum constants for each demographic is 2-3 times larger in the imbalanced model than in the balanced model.

1. **Effectiveness of Obfuscation: How does the effectiveness of face obfuscation systems vary with population demographics?** Our findings indicate that the metric embedding network is less robust for samples from minority demographic groups; the strength of the perturbation necessary to change the identity is smaller than for samples from majority demographic groups. Disparities are evident between demographics in both the targeted and untargeted cases, and this gap widens for source-target pairs of the same demographic group. We find that perturbations, especially those with smaller ℓ_p norm, lose some of their advantage after transferring onto a black-box model.
2. **Utility of Face Obfuscation: How does the clustering of the embedding space impact the utility of face obfuscation?** Our main takeaway is that perturbed faces retain their original demographic attribute. Stronger perturbations are required to target an identity of a different demographic group than to target an identity of the same demographic group. We also observe the embeddings of the untargeted perturbed faces to overlap those of the natural faces.
3. **Dataset Balancing: How does the balance of training set demographics impact the utility of face obfuscation?** We observe that a ResNet-18 trained on a sex-balanced VGGFace2 dataset is not only more robust compared to a standard VGGFace2 trained ResNet-18 model, it also reduces the performance gap between demographics in face obfuscation systems.

6.1 Experimental Setup

Datasets and Models: We utilize the LFW and VGGFace2 datasets in the rest of this evaluation; these datasets are described earlier in section 5.1. In the white-box setting, we generate perturbed faces using the FaceNet Model, which was also described earlier in section 5.1. In the black-box setting, we test for the transferability of the perturbed faces to the Face++ face recognition API [40] or a pre-trained OpenFace model [41]. The OpenFace model is another, smaller Inception ResNet network; it is trained using triplet loss on $96 \times 96 \times 3$ images and is tuned to output 128-dimension embeddings. Trained on both the CASIA-WebFace [42] and FaceScrub [43] datasets, it achieves a 0.973 area under the curve (AUC) on the LFW dataset.

Attacks: We perform our evaluation using untargeted and targeted variants of facial obfuscation systems, as described in section 3. For the targeted case, we generate adversarial examples with a subset of the

LFW [5] dataset, the FaceNet [3] model, and the Face-off implementation [7]. We used 0, 5, and 10 as our margin values (κ in eq. (7)). We generated untargeted attacks using the Lowkey [8] attack as described in section 3.3. The ensemble used in the LowKey attack includes two pre-trained ArcFace models [4] and two pre-trained Cosface models [44]. We report the obfuscation success rate as an indicator of the perturbation’s effectiveness. In the targeted case, it measures the proportion of perturbed faces which match their intended targets. In the untargeted case, it measures the proportion of perturbed faces that evade their source identity. **Scenarios:** We consider six demographic attributes, four for race (Black, White, Indian, Asian) and two for sex (female, male). We sample 50 identities per attribute from the LFW dataset². We do not condition on the number of images per identity. Thus, some demographics may have more average images per identity than others, though this disparity is not large. We refer to these images as the source images, and we use them as inputs to the untargeted attack. For the targeted attacks, we create two scenarios:

- Same demographic: We choose 49 pairwise combinations of target identities from the same race/sex for each source identity. This sampling leads to 2450 source-target pairs of the same sex and 2450 source-target pairs of the same race.
- Different demographic: We subsample – uniformly at random – 15 target identities from each different race for a total of 45 target identities, and 50 target identities from the opposite sex. This sampling leads to 2250 source-target pairs of the different races and 2500 source-target pairs of the different sex.

We generate untargeted adversarial examples for each of the 5,749 identities in the LFW dataset and their associated images. We generate targeted adversarial examples for earlier scenario’s 300 non-unique identities and 80,000+ targeted examples corresponding to the 28,700 pairs of identities.

6.2 Effectiveness of Obfuscation

Methodology: This question is addressed with three experiments, each tackling an important component of face obfuscation systems. In our attack scenarios, we are interested in understanding how the strength of generated perturbations differs with each demographic group. Our first experiment examines the distributions of ℓ_2 norms for each perturbation conditioned on demographic attributes. The second experiment measures obfuscation success in terms of both untargeted and targeted obfuscation success rates. The last of the experiments evaluates these success metrics in the black-box setting.

Results and Discussion: Using the adversarial examples generated from the targeted attack, we examine the distribution of perturbation norms conditioned by demographic attribute. The perturbation norms appear smaller for same demographic pairs than for different demographic pairs in fig. 6. This result is consistent with the discussion about Lipschitz constants in section 5.4. Users wishing to mask their faces in a less visible manner may gravitate towards selecting a target identity of the same race or sex. However, this might be counterproductive to the user’s privacy for two reasons: 1) adversarial perturbations with smaller ℓ_p norms will struggle in transferring to other models and 2) users who perturb within the same demographic may leak demographic information to our online adversary.

In the case of the targeted adversarial examples, we also observe the effectiveness to be dependent on the demographic attribute. In fig. 7, the faces with the White race attribute exhibit a clear edge over the other races with a clearly higher obfuscation rate. When performing the black-box evaluation on the OpenFace model, we observe a similar trend. When transferring onto another model, the examples lose some of their attack strength. Examples generated on faces from the majority group still transfer better than those of minority groups. We conjecture that the larger perturbation norms of such faces contribute

²The LFW demographic attributes were annotated using binary attribute and simile classifiers [20].

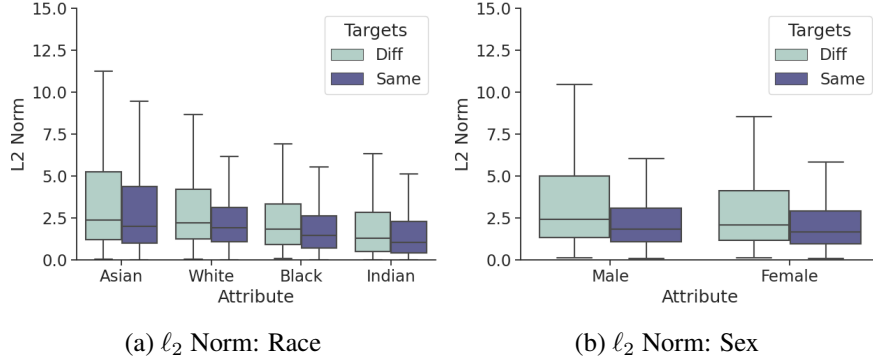
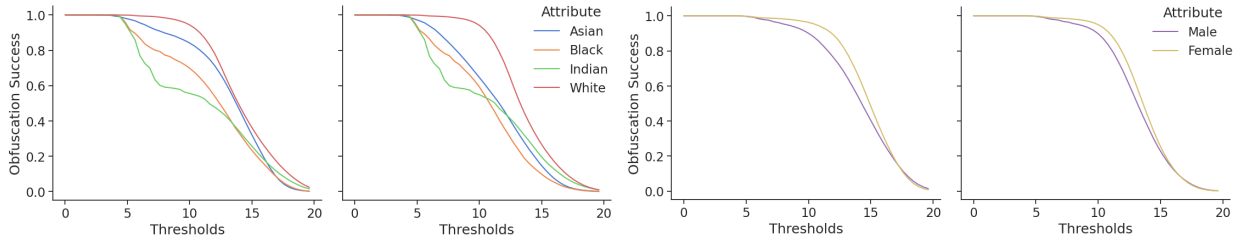


Figure 6: The ECDF of adversarial perturbation sizes generated using the CW [45] attack. Along with the disparity among demographics, the perturbation sizes tend to be smaller for attack pairs of the same demographic.



(a) Targeted: Different Race (Left) vs. Same Race (Right) (b) Targeted: Different Sex (Left) vs. Same Sex (Right)

Figure 7: Targeted obfuscation success evaluated on FaceNet in a white-box setting.

to improved transferability rates. This observation is consistent with an observation from Face-off [7]; amplifying perturbations improved transferability to black-box models.

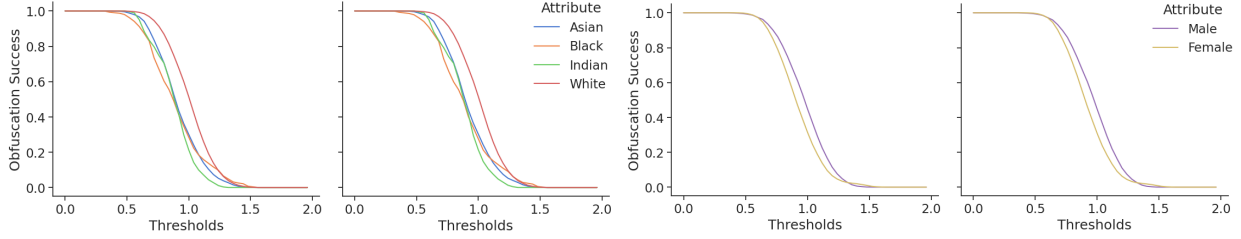
When repeating the above evaluation for the untargeted case, we do not observe much discrepancy in terms of the size of perturbations or success rates among different demographics. Still, demographic attributes influence the behavior of untargeted obfuscation systems as we observe later.

Finally, we tested the success of the perturbed faces against the Face++ face recognition API. In fig. 9, we present the distribution of the obfuscation success rate in the untargeted case. For race, we observe higher success rates for White and Asian faces. It is also worth noting in fig. 5 and fig. 6, that Asian faces also perform similarly to White faces. Meanwhile, Indian and Black faces suffer from less robustness in the network, decreased perturbation sizes, and lower obfuscation success rate. While Asian faces are also a minority in the training set, we observe a large variation in their results. We attribute the reason for some Asian faces having a lighter skin tone than the other races, as evident from fig. 4. Similarly, for the sex attribute, we observe a slightly higher success rate for the male faces.

6.3 Utility of Face Obfuscation

Methodology: We analyze whether face obfuscation systems alter demographic information encoded within the face. This analysis is important to the real-world utility of face obfuscation systems. If the user cannot alter their demographic attributes, they leak part of their identity to the service provider. In the targeted case, this can occur if a user cannot successfully attack a target from a different demographic. It can additionally occur in the untargeted case if the adversarial examples retain the source demographic.

For the untargeted adversarial examples, we pass the perturbed faces through a classifier that predicts the



(a) Targeted: Different Race (Left) vs. Same Race (Right) (b) Targeted: Different Sex (Left) vs. Same Sex (Right)

Figure 8: Targeted obfuscation success evaluated on OpenFace in a black-box setting.

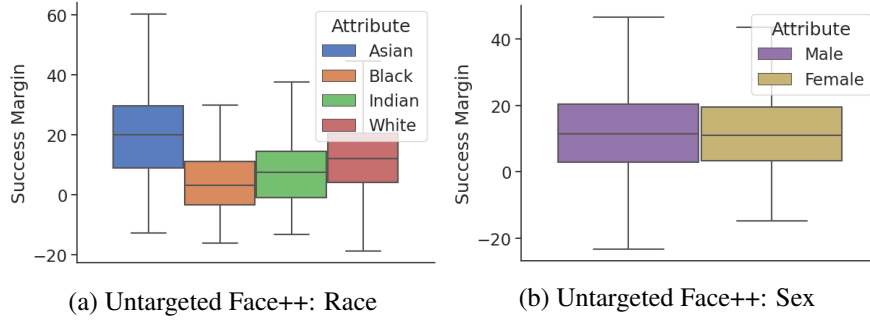


Figure 9: Untargeted adversarial examples generated using LowKey [8] and evaluated on Face++.

race attribute from a face [46]. This classifier is trained using the VGG-Face face recognition model [47] as the base; the last seven layers are fine-tuned with a softmax to predict race facial attributes on the FairFace dataset [48]. Originally, this classifier predicts six labels for race: Asian, Indian, Black, Middle Eastern, Latino, and White. However, our LFW dataset does not contain Middle Eastern and Latino label as a ground truth. Since the classifier has higher confusion with White, Middle Eastern, and Latino labels³, we combine these labels into one “White” label. As such, the classifier predicts between four labels: Asian, Indian, Black, and White. We compare the predicted race of the perturbed image to the actual race of the source image. Finally, we visualize the t-SNE embeddings of the natural and adversarial examples conditioned on their demographic attribute. To evaluate the examples from a black-box perspective, we generate the t-SNE embeddings on the FaceNet model. The adversarial examples are generated with the ensemble of models used in LowKey.

Results and Discussion: For the targeted case, we analyze the same demographic and different demographic scenarios as shown in figs. 6 and 7. First, we look at the differences in the perturbation norms from figs. 6a and 6b. It is clear from the figure, for both sex and race attributes, that the ℓ_p norms of the perturbations are higher in the different demographic scenario than the same demographic scenario. For each race and sex attribute, it is easier to perturb the face when the target has the same demographic attribute; this refers to the size of perturbation being smaller. As such, the user of the face obfuscation system suffers in utility when they choose a target of different demographic attribute.

Further, we examine the obfuscation success rate when the user chooses a target from their own demographic compared to the case of different demographic. For this purpose, we compare the left and right plots of figs. 7a and 7b. For each demographic attribute, the success rate is slightly higher when the target is of the different group. We observe a minute difference in the transferability results from figs. 8a and 8b. The success rate can be attributed to the increased perturbation strength (fig. 6) when the target is from a

³<https://sefiks.com/2019/11/11/race-and-ethnicity-prediction-in-keras/>

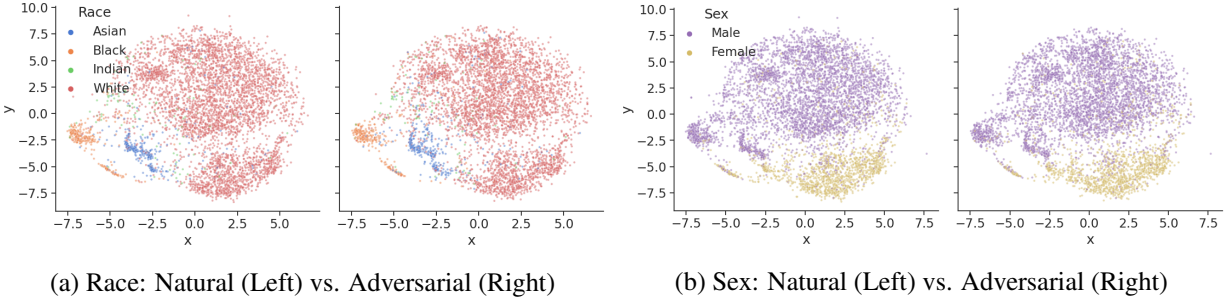


Figure 10: t-SNE [18] of the embedding spaces generated using the non-adversarial and untargeted adversarial LFW [5] datasets. Embeddings of identities are colored by race and sex. Note that the clusters do not change, identities are still rooted within their own demographic.

different demographic group.

For the untargeted case, the race classifier yields a 92% matching rate between the predicted race of the adversarial image and the source image. This result indicates that while an untargeted attack can change the predicted identity, it retains the original race attribute. Note that the race classifier is not adversarially trained, and is not aware of possible face obfuscation taking place.

In fig. 10, we visualize the t-SNE embedding of the natural examples and adversarial examples based on their source demographics. Comparing the left and right plots of figs. 10a and 10b, it is clear that the embeddings of the adversarial examples overlap with those of the natural examples of the same race. The same is true for fig. 10b. These results further confirm our intuition from section 4.4; an adversarial perturbation does not push away the sample from its demographic group, when the groups are clustered.

6.4 Balancing the Dataset

Methodology: We train two metric embedding networks, which have the ResNet-18 architecture. The first network is trained on the entirety of the VGGFace2 [6] dataset’s training split, a total of 8631 identities. Since VGGFace2 contains roughly 60%/40% male/female images, we create a second training benchmark upon which we train a metric embedding network. This second dataset, henceforth referred to as Sex Balanced VGGFace2, contains a total of 4866 identities. The Sex Balanced VGGFace2 dataset was created by removing original identities to create a training set which contains an equal number identities for the demographic of interest. We choose to remove examples from VGGFace2 to data augmentation so that we do not introduce any artifacts potentially introduced by the latter. Using the same training regime, we obtain a Sex Balanced ResNet-18 and a standard ResNet-18 (sex imbalanced). Because we wish to avoid augmenting VGGFace2 with synthetic examples, we drop identities from the male group. Unfortunately, creating a Race Balanced VGGFace2 would remove 80% of the identities since the imbalance is much more extreme in this case. It would be unclear whether changes in performance would be attributed to the dataset size or the balancing of identities.

The balanced accuracy⁴ (when measured on the LFW dataset) of the model trained on the standard set is 0.33 and that of the model trained on the Sex Balanced set is 0.31. While the balanced accuracy of these models is low (we discuss in section 7), the model clearly distinguishes between female and male faces. We are interested in this group-based behavior of the model as to compare the demographic disparities of the face obfuscation; we run the attacks only on faces on which the model performs well.

Results and Discussion: After training a Sex Balanced and a standard ResNet-18, we evaluate the

⁴The balanced accuracy [49, 50] is the sum of true positive and true negative rates of a thresholded nearest neighbors classifier divided by 2.

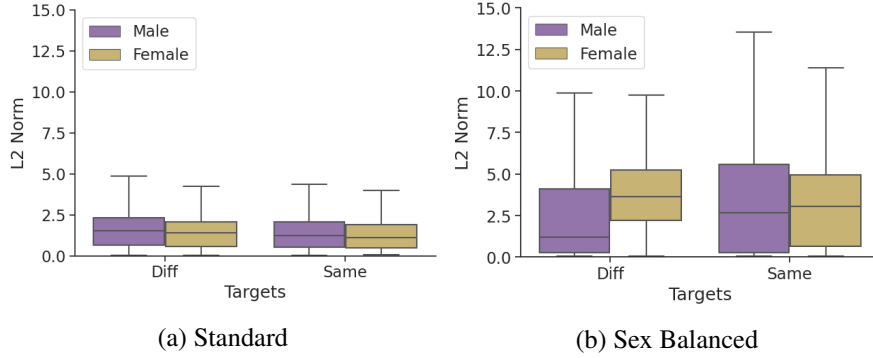


Figure 11: The ECDF of adversarial perturbation sizes generated using the CW [45] attack on the balanced and standard models. The balanced model appears more robust requiring larger perturbations. Disparities in perturbation sizes exist between Male and Female.

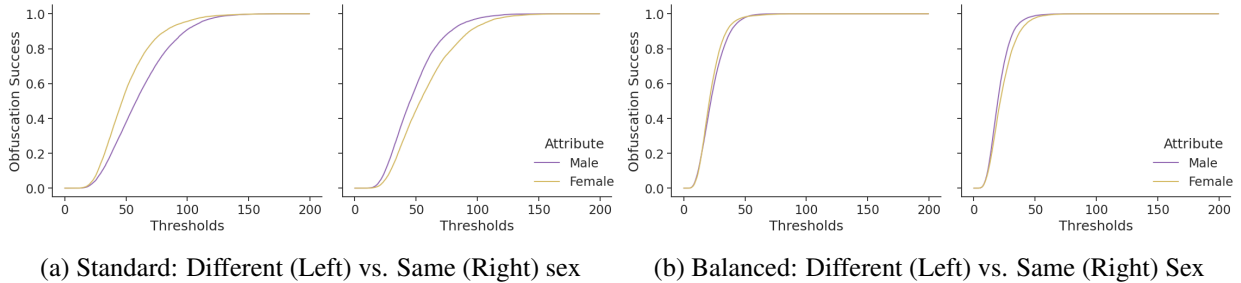


Figure 12: Untargeted obfuscation success on ResNet18 models in a white-box setting. Generating examples on the balanced model closes the performance gap and improves success.

adversarial robustness of both models. We once more compare the strength of the perturbations in both models. In fig. 11, our results indicate the Sex Balanced model is more robust to adversarial attacks; the resulting perturbations are larger for both demographic groups than the imbalanced case. This finding is consistent with our previous discussion about the robustness of the network and local Lipschitz constants. In fig. 5, we show how balancing the dataset lowers the estimated local Lipschitz constants. As we previously observed, the increased perturbation strength makes the adversarial examples more transferable.

Figure 12 reports the obfuscation success rate for the targeted attacks; these attacks are generated in the white-box setting. As evident from the plots, there is a discrepancy in the obfuscation success rate between the female and male attributes. In the same sex scenario (fig. 12a-right), the obfuscation success rate of male faces outperforms that of female faces, which is opposite to the different sex scenario (fig. 12a-left). After balancing the dataset, the gaps between the male and female users diminish (fig. 12b). It is important to note that these results are for the white-box setting; balancing the training datasets does not guarantee fairness. The demographic discrepancies still exist when applying these perturbed examples to the black-box setting (fig. 15).

7 Discussion

In this section, we discuss the main insights about the performance of obfuscation systems and their demographic disparities. We draw these insights from the analytical model of section 4 and evaluations of both section 5 and section 6.

7.1 Implications of Our Work

Our findings suggest that face obfuscation systems are not one-dimensional attacks; demographic dimensions factor into privacy risks induced by face obfuscation. These systems, which rely on evasion attacks, maintain poor performance and leak information, especially for minority demographics. We have observed that users from minority groups suffer a lower obfuscation rate and cannot choose target identities outside their groups. As such, we call the fairness properties of such systems into question as their performance differs between individuals belonging to different demographic groups.

7.2 Extending Theory to Real-World Systems

Using a k -component PCA as a proxy for large-scale embedding networks, we developed an analytical model to characterize face recognition and obfuscation systems. We were able to characterize how embedding networks might fail to capture information in images corresponding to demographic subgroups, which make a small contribution to the overall variation in data. Often, this result means that demographic subgroups, consisting of fewer samples, suffer poorer performance when utilizing face obfuscation systems. In addition to our performance analysis of face obfuscation systems, we show that a given image requires stronger adversarial perturbations to register as a different demographic. This case is especially prominent for members of minority groups.

7.3 Race and Skintones

We observe that conditioning by race yields slightly different conclusions than conditioning by sex. Whereas the set of facial features and skin tones used to predict the race of an individual can overlap, there is sexual dimorphism apparent in the labeling of human faces [51–53]. For example, we observe, on average, faces labeled as White, Middle Eastern, Latino, and Asian tend to have lighter skin, whereas Black and Indian tend to have darker skin tones. Hence, in our analysis, it is notable that faces of Asian and White groups perform similarly while faces of the Black and Indian groups perform similarly. Even in the case of skin tone, there is significant variance. The skin tone of a person may vary with lighting conditions or change naturally over time.

7.4 Potential Remedies

We have discussed how disparities in the demographic distributions of the training set can significantly impact face obfuscation performance. However, this is not an easily solvable problem. Finding a diverse large-scale dataset to train face recognition models has proven difficult. Datasets, such as FairFace [48] and IBM’s Diversity in Faces [54], attempt to address this problem. But, as seen in our experiments, balancing demographics in a dataset is not straightforward. There is a need to define a proper methodology for balancing demographics across datasets. Even if one creates an even proportion of demographics, some demographic attributes such as skin tone can overlap across races. Additionally, users may be interested in combinations of different demographic attributes, which are difficult to balance in practice. Serna et al. propose Sensitive Loss, a “discrimination-aware” Triplet Loss derived tuning procedure for pre-trained models [55]. This tuning procedure involves adding an additional layer to the network, then tweaking this layer using only identities drawn from the same demographic group.

However, remedying the data imbalance effects partially addresses the demographic disparities in facial obfuscation. Demographic imbalances in the evaluation set, such as a friends list on social media, can affect even a balanced model. We evaluate this effect by simulating the top- k accuracy of the Sex Balanced ResNet-18 in a nearest-neighbors setting; the top- k accuracy metric denotes whether the correct identity of a perturbed face belongs to the set of the top- k matching faces from a bucket of embeddings. We simulate



Figure 13: Higher top- k accuracy is equivalent to lower privacy utility; left: imbalanced training, right: balanced training.

three simple scenarios a user might encounter on a social media site: the obfuscated face belongs to the minority demographic of the friend/follower group (K -minority), the majority demographic (K -majority), or if the demographics are balanced (balance). As evident in fig. 13-right, the face obfuscation system is much less effective on faces that belong to the K -minority demographic than those belonging to the K -majority demographic; a user from a minority group has a higher chance of being re-identified in this setting, even if the training set is balanced and the face obfuscation system is more fair.

7.5 Threats to Validity

We discuss some of the limitations of our analytical and experimental approaches. First, our intention for section 4 is to create an analytical model for embedding spaces and dimensionality reduction in general. We focus on PCA in our model, though we intend to extend the results to other machine learning systems, including deep neural networks. PCA is a linear embedding function and is incapable of capturing non-linear effects. For example, the construction of PCA means there is no difference in local Lipschitz constants when conditioned on demographic groups. Second, our results involving training balanced and imbalanced models to obtain local Lipschitz constants is only an approximation, as the non-linear activation functions of large-scale neural networks are computationally complex. The evaluated networks are also not metric embedding networks but are small classification models. Estimating local Lipschitz constant on large embedding networks is infeasible given the current estimators.

Second, the number of benchmark datasets we use are limited. Publicly available facial recognition datasets are scarce, and datasets with labeled demographic attributes are even harder to come by. Such publicly available datasets are rather small, on the order of thousands of identities. As such, our results may not generalize to datasets orders of magnitude larger than currently available facial recognition datasets.

Lastly, we note how training metric embedding networks is computationally expensive. Whereas classification networks are trained on labeled examples, metric embedding networks are trained tuples of labeled examples. As such, the time to train may metric embedding network has a stronger dependence on the number of training examples instead of the linear dependence on training examples seen when training classification networks. Consequently, most of our analysis relies on pre-trained models, such as FaceNet and OpenFace. We only train small embedding networks to evaluate the balancing of the dataset in section 6.4. These computational limitations contribute to the relatively lower accuracy of the ResNet-18 when trained on the Sex Balanced VGGFace2 and the default VGGFace2 datasets.

8 Related Work

Researchers have recently started looking into the intersection of facial recognition and machine learning fairness. Buolamwini and Gebru study commercially available facial recognition datasets and classifiers [14]. Their findings indicate three commercial face classifiers, across all three benchmark datasets, have disparate performance across demographic subgroups. Follow-up research has attempted to address these demographic disparities through balanced datasets [48, 56]. Such datasets improve the generalization performance but do not address demographic disparities completely. These findings are consistent with our results in section 6, where we observe that a demographically balanced dataset may still contain biases towards specific attributes such as skin tone.

More related to our research, Nanda et al. discuss the relationship between fairness and robustness of facial recognition [15]. They show that faces from minority groups require smaller adversarial perturbations to misclassify compared to those for majority groups; this discrepancy is a factor of the underlying datasets, models, and hyperparameter tuning. Our work differs along three dimensions. First, we study the robustness of facial recognition in the context of the metric embedding networks – the real-world setting for such systems. Second, we present an empirical characterization of face obfuscation systems that build on evasion attacks; our characterization extends beyond the perturbation size to the success rate in white-box and black-box settings. Further, we study the real-world implications of demographic disparities of facial obfuscation systems, which prevent a user from choosing targets outside their demographic group. Third, we present an analytical model of an embedding function to reason about the robustness of facial recognition and obfuscation systems. Finally, a master thesis by Qin [57] evaluates the performance discrepancies in the FAWKES [30] conditioned on skin tones. FAWKES is a data poisoning-based technique for face obfuscation. Using DSSIM similarity scores, Qin finds differences in perturbation visibility for certain demographics. In comparison, our work characterizes why these discrepancies exist in the adversarial setting and how they impact the privacy utility of all face obfuscation systems.

9 Conclusion

Face recognition systems have seen increased usage in online and physical settings at the cost of heightened privacy concerns. Researchers have proposed face obfuscation systems that leverage evasion attacks against metric embedding networks. Our results show that, in an effort to mitigate such privacy concerns, face obfuscation systems have performance characteristics that depend on demographic information, thereby creating a new privacy incursion. These characteristics can not only leak demographic membership information, but also decrease the performance of face obfuscation among underrepresented demographic groups. Imbalances in the demographics of a training regime are indicative of the root of these privacy utility issues. To mitigate the effects of this incidental privacy leak, we must not only develop loss functions for training fair metric embedding networks, but also develop techniques to characterize if such privacy leaks will occur.

References

- [1] L. Feiner and A. Palmer, “Rules around facial recognition and policing remain blurry,” *CNBC Tech*, 2021.
- [2] A. Roussi, “Resisting the rise of facial recognition,” *Nature*, 2020.
- [3] F. Schroff, D. Kalenichenko, and J. Philbin, “FaceNet: A unified embedding for face recognition and clustering,” in *Proceedings of the IEEE conference on computer vision and pattern recognition*, 2015, pp. 815–823.
- [4] J. Deng, J. Guo, X. Niannan, and S. Zafeiriou, “Arcface: Additive angular margin loss for deep face recognition,” in *CVPR*, 2019.
- [5] G. B. Huang, M. Ramesh, T. Berg, and E. Learned-Miller, “Labeled faces in the wild: A database for studying face recognition in unconstrained environments,” University of Massachusetts, Amherst, Tech. Rep. 07-49, October 2007.
- [6] Q. Cao, L. Shen, W. Xie, O. M. Parkhi, and A. Zisserman, “Vggface2: A dataset for recognising faces across pose and age,” in *2018 13th IEEE international conference on automatic face & gesture recognition (FG 2018)*. IEEE, 2018, pp. 67–74.
- [7] V. Chandrasekaran, C. Gao, B. Tang, K. Fawaz, S. Jha, and S. Banerjee, “Face-off: Adversarial face obfuscation,” *CoRR*, vol. abs/2003.08861, 2020. [Online]. Available: <https://arxiv.org/abs/2003.08861>
- [8] V. Cherepanova, M. Goldblum, H. Foley, S. Duan, J. P. Dickerson, G. Taylor, and T. Goldstein, “Lowkey: Leveraging adversarial attacks to protect social media users from facial recognition,” *CoRR*, vol. abs/2101.07922, 2021. [Online]. Available: <https://arxiv.org/abs/2101.07922>
- [9] I. Evtimov, P. Sturmfels, and T. Kohno, “FoggySight: A scheme for facial lookup privacy,” in *2021 Proceedings on Privacy Enhancing Technologies*. PoPETs, 2021.
- [10] I. J. Goodfellow, J. Shlens, and C. Szegedy, “Explaining and harnessing adversarial examples,” *arXiv preprint arXiv:1412.6572*, 2014.
- [11] A. Madry, A. Makelov, L. Schmidt, D. Tsipras, and A. Vladu, “Towards deep learning models resistant to adversarial attacks,” *arXiv preprint arXiv:1706.06083*, 2017.
- [12] N. Carlini and D. Wagner, “Towards evaluating the robustness of neural networks,” in *2017 IEEE Symposium on Security and Privacy (SP)*, 2017, pp. 39–57.
- [13] E. Radiya-Dixit and F. Tramèr, “Data poisoning won’t save you from facial recognition,” in *ICML Workshop on Adversarial Machine Learning (AdvML)*, 2021. [Online]. Available: <https://arxiv.org/abs/2106.14851>
- [14] J. Buolamwini and T. Gebru, “Gender shades: Intersectional accuracy disparities in commercial gender classification,” in *Conference on Fairness, Accountability and Transparency, FAT 2018, 23-24 February 2018, New York, NY, USA*, ser. Proceedings of Machine Learning Research, S. A. Friedler and C. Wilson, Eds., vol. 81. PMLR, 2018, pp. 77–91. [Online]. Available: <http://proceedings.mlr.press/v81/buolamwini18a.html>

- [15] V. Nanda, S. Dooley, S. Singla, S. Feizi, and J. P. Dickerson, “Fairness through robustness: Investigating robustness disparity in deep learning,” in *Proceedings of the 2021 ACM Conference on Fairness, Accountability, and Transparency*, ser. FAccT ’21. New York, NY, USA: Association for Computing Machinery, 2021, p. 466–477. [Online]. Available: <https://doi.org/10.1145/3442188.3445910>
- [16] H. Zhang, P. Zhang, and C.-J. Hsieh, “Recurjac: An efficient recursive algorithm for bounding jacobian matrix of neural networks and its applications,” in *AAAI Conference on Artificial Intelligence (AAAI)*, *arXiv preprint arXiv:1810.11783*, dec 2019.
- [17] B. Kim, M. Wattenberg, J. Gilmer, C. Cai, J. Wexler, F. Viegas, and R. sayres, “Interpretability beyond feature attribution: Quantitative testing with concept activation vectors (TCAV),” in *Proceedings of the 35th International Conference on Machine Learning*, ser. Proceedings of Machine Learning Research, J. Dy and A. Krause, Eds., vol. 80. PMLR, 10–15 Jul 2018, pp. 2668–2677. [Online]. Available: <http://proceedings.mlr.press/v80/kim18d.html>
- [18] L. van der Maaten and G. Hinton, “Visualizing data using t-sne,” *Journal of Machine Learning Research*, vol. 9, pp. 2579–2605, 11 2008.
- [19] F. Tramèr, N. Papernot, I. Goodfellow, D. Boneh, and P. McDaniel, “The Space of Transferable Adversarial Examples,” *ArXiv e-prints*, Apr. 2017.
- [20] N. Kumar, A. C. Berg, P. N. Belhumeur, and S. K. Nayar, “Attribute and Simile Classifiers for Face Verification,” in *IEEE International Conference on Computer Vision (ICCV)*, Oct 2009.
- [21] K. P. F.R.S., “Liii. on lines and planes of closest fit to systems of points in space,” *The London, Edinburgh, and Dublin Philosophical Magazine and Journal of Science*, vol. 2, no. 11, pp. 559–572, 1901. [Online]. Available: <https://doi.org/10.1080/14786440109462720>
- [22] G. E. Hinton and S. Roweis, “Stochastic neighbor embedding,” in *Advances in Neural Information Processing Systems*, S. Becker, S. Thrun, and K. Obermayer, Eds., vol. 15. MIT Press, 2003. [Online]. Available: <https://proceedings.neurips.cc/paper/2002/file/6150ccc6069bea6b5716254057a194ef-Paper.pdf>
- [23] S. Barocas, M. Hardt, and A. Narayanan, *Fairness and Machine Learning*. fairmlbook.org, 2019, <http://www.fairmlbook.org>.
- [24] C. Dwork, M. Hardt, T. Pitassi, O. Reingold, and R. Zemel, “Fairness through awareness,” in *Proceedings of the 3rd Innovations in Theoretical Computer Science Conference*, ser. ITCS ’12. New York, NY, USA: Association for Computing Machinery, 2012, p. 214–226. [Online]. Available: <https://doi.org/10.1145/2090236.2090255>
- [25] A. Holmes, “533 million facebook users’ phone numbers and personal data have been leaked online,” *Business Insider Tech*, 2021.
- [26] D. Harwell, “This facial recognition website can turn anyone into a cop — or a stalker,” May 2021. [Online]. Available: <https://www.washingtonpost.com/technology/2021/05/14/pimeyes-facial-recognition-search-secrecy/>
- [27] G. Greenwald, “Nsa collecting phone records of millions of verizon customers daily,” Jun 2013. [Online]. Available: <https://www.theguardian.com/world/2013/jun/06/nsa-phone-records-verizon-court-order>

- [28] J. Swan, “Tucker carlson sought interview with putin at time of nsa spying claim,” Jul 2021. [Online]. Available: <https://www.axios.com/tucker-carlson-putin-interview-surveillance-c9952d7c-33d7-45e9-be68-2ba4c3817f98.html>
- [29] M. Sharif, S. Bhagavatula, L. Bauer, and M. K. Reiter, “Accessorize to a crime: Real and stealthy attacks on state-of-the-art face recognition,” in *Proceedings of the 2016 ACM SIGSAC Conference on Computer and Communications Security*. ACM, 2016, pp. 1528–1540.
- [30] S. Shan, E. Wenger, J. Zhang, H. Li, H. Zheng, and B. Y. Zhao, “Fawkes: Protecting privacy against unauthorized deep learning models,” in *29th USENIX Security Symposium, USENIX Security 2020, August 12-14, 2020*, S. Capkun and F. Roesner, Eds. USENIX Association, 2020, pp. 1589–1604. [Online]. Available: <https://www.usenix.org/conference/usenixsecurity20/presentation/shan>
- [31] R. Zhang, P. Isola, A. A. Efros, E. Shechtman, and O. Wang, “The unreasonable effectiveness of deep features as a perceptual metric,” in *CVPR*, 2018.
- [32] J. D’Orazio, S. Jarrett, A. Amaro-Ortiz, and T. Scott, “Uv radiation and the skin,” *International journal of molecular sciences*, vol. 14, no. 6, pp. 12 222–12 248, Jun 2013. [Online]. Available: <https://pubmed.ncbi.nlm.nih.gov/23749111>
- [33] P. Bartlett, D. J. Foster, and M. Telgarsky, “Spectrally-normalized margin bounds for neural networks,” *arXiv preprint arXiv:1706.08498*, 2017.
- [34] B. Neyshabur, S. Bhojanapalli, D. McAllester, and N. Srebro, “Exploring generalization in deep learning,” *arXiv preprint arXiv:1706.08947*, 2017.
- [35] K. Scaman and A. Virmaux, “Lipschitz regularity of deep neural networks: analysis and efficient estimation,” *arXiv preprint arXiv:1805.10965*, 2018.
- [36] T.-W. Weng, H. Zhang, P.-Y. Chen, J. Yi, D. Su, Y. Gao, C.-J. Hsieh, and L. Daniel, “Evaluating the robustness of neural networks: An extreme value theory approach,” *arXiv preprint arXiv:1801.10578*, 2018.
- [37] U. V. Luxburg and O. Bousquet, “Distance-based classification with lipschitz functions,” in *J. Mach. Learn. Res.*, 2003.
- [38] T.-W. Weng, H. Zhang, H. Chen, Z. Song, C.-J. Hsieh, D. Boning, and I. S. D. A. Daniel, “Towards fast computation of certified robustness for relu networks,” in *International Conference on Machine Learning (ICML)*, july 2018.
- [39] K. Simonyan and A. Zisserman, “Very deep convolutional networks for large-scale image recognition,” in *International Conference on Learning Representations*, 2015.
- [40] Face++, “Face++,” <https://www.faceplusplus.com>.
- [41] B. Amos, B. Ludwiczuk, and M. Satyanarayanan, “Openface: A general-purpose face recognition library with mobile applications,” CMU-CS-16-118, CMU School of Computer Science, Tech. Rep., 2016.
- [42] D. Yi, Z. Lei, S. Liao, and S. Z. Li, “Learning face representation from scratch,” *arXiv preprint arXiv:1411.7923*, no. 11, 2014.
- [43] H.-W. Ng and S. Winkler, “A data-driven approach to cleaning large face datasets,” in *2014 IEEE International Conference on Image Processing (ICIP)*, 2014, pp. 343–347.

- [44] H. Wang, Y. Wang, Z. Zhou, X. Ji, D. Gong, J. Zhou, Z. Li, and W. Liu, “Cosface: Large margin cosine loss for deep face recognition,” in *2018 IEEE/CVF Conference on Computer Vision and Pattern Recognition*, 2018, pp. 5265–5274.
- [45] N. Carlini and D. Wagner, “Towards evaluating the robustness of neural networks,” in *2017 IEEE Symposium on Security and Privacy (SP)*. IEEE, 2017, pp. 39–57.
- [46] S. I. Serengil and A. Ozpinar, “Lightface: A hybrid deep face recognition framework,” in *2020 Innovations in Intelligent Systems and Applications Conference (ASYU)*. IEEE, 2020, pp. 23–27.
- [47] O. M. Parkhi, A. Vedaldi, and A. Zisserman, “Deep face recognition,” in *British Machine Vision Conference*, 2015.
- [48] K. Karkkaine and J. Joo, “Fairface: Face attribute dataset for balanced race, gender, and age,” *arXiv:1908.04913 [cs.CV]*, 2019.
- [49] K. H. Brodersen, C. S. Ong, K. E. Stephan, and J. M. Buhmann, “The balanced accuracy and its posterior distribution,” in *2010 20th International Conference on Pattern Recognition*, 2010, pp. 3121–3124.
- [50] L. Mosley, “A balanced approach to the multi-class imbalance problem,” Ph.D. dissertation, Iowa State University, 2013.
- [51] A. C. Little, B. C. Jones, C. Waitt, B. P. Tiddeman, D. R. Feinberg, D. I. Perrett, C. L. Apicella, and F. W. Marlowe, “Symmetry is related to sexual dimorphism in faces: Data across culture and species,” *PLOS ONE*, vol. 3, no. 5, pp. 1–8, 05 2008. [Online]. Available: <https://doi.org/10.1371/journal.pone.0002106>
- [52] D. I. Perrett, K. J. Lee, I. Penton-Voak, D. Rowland, S. Yoshikawa, D. M. Burt, S. Henzi, D. L. Castles, and S. Akamatsu, “Effects of sexual dimorphism on facial attractiveness,” *Nature*, vol. 394, no. 6696, pp. 884–887, 1998.
- [53] K. Kleisner, P. Tureček, S. C. Roberts, J. Havlíček, J. V. Valentova, R. M. Akoko, J. D. Leongómez, S. Apostol, M. A. Varela, and S. A. Saribay, “How and why patterns of sexual dimorphism in human faces vary across the world,” *Scientific reports*, vol. 11, no. 1, pp. 1–14, 2021.
- [54] M. Merler, N. Ratha, R. S. Feris, and J. R. Smith, “Diversity in faces,” 2019.
- [55] I. Serna, A. Morales, J. Fierrez, M. Cebrian, N. Obradovich, and I. Rahwan, “Sensitiveloss: Improving accuracy and fairness of face representations with discrimination-aware deep learning,” 2020.
- [56] B. Thomee, D. A. Shamma, G. Friedland, B. Elizalde, K. Ni, D. Poland, D. Borth, and L.-J. Li, “Yfcc100m: The new data in multimedia research,” *Commun. ACM*, vol. 59, no. 2, p. 64–73, Jan. 2016. [Online]. Available: <https://doi.org/10.1145/2812802>
- [57] S. Qin, “Bias and fairness of evasion attacks in image perturbation,” Master’s thesis, Central Washington University, 2021.

A Supplemental Mathematics for the Analytical Model

In this section we provide additional results for our analytical model as described in section 4.1

A.1 Important Lemmas and Identities

Lemma A.1.1 (Law of Total Variance). *Let X and Y be random variables in the same probability space. Furthermore, let the variance of both X and Y be finite, then*

$$\text{Var}(Y) = \mathbb{E}[\text{Var}(Y | X)] + \text{Var}(\mathbb{E}[Y | X]) \quad (12)$$

Lemma A.1.2 (Law of Total Covariance). *Let X , Y and Z be random variables in the same probability space. Furthermore, let the covariance of X and Y be finite, then*

$$\begin{aligned} \text{cov}(X, Y) &= \mathbb{E}[\text{cov}(X, Y | Z)] \\ &\quad + \text{cov}(\mathbb{E}[X | Z], \mathbb{E}[Y | Z]) \end{aligned} \quad (13)$$

A.2 Decomposing the Covariance

Let us compute the diagonal components of the overall covariance matrix Σ of synthetic data distribution \mathcal{D} in terms of Σ_a, Σ_b the covariance matrices for identity distributions \mathcal{D}_a and \mathcal{D}_b , respectively:

$$(\Sigma)_{jj} = \alpha_a(\Sigma_a)_{jj} + (1 - \alpha_a)(\Sigma_b)_{jj} + \alpha_a((\mu_a)_j - (\mu_{ab})_{jj})^2 + (1 - \alpha_a)((\mu_b)_j - (\mu_{ab})_{jj})^2 \quad (14)$$

$$= \alpha_a(\Sigma_a)_{jj} + (1 - \alpha_a)(\Sigma_b)_{jj} + \alpha_a(1 - \alpha_a)((\mu_a)_j - (\mu_b)_j)^2 \quad (15)$$

Now we compute the off-diagonal components of the overall covariance matrix Σ in terms of Σ_a and Σ_b :

$$\begin{aligned} (\Sigma)_{jk} &= \alpha_a(\Sigma_a)_{jk} + (1 - \alpha_a)(\Sigma_b)_{jk} \\ &\quad + \alpha_a\left((\mu_a)_j - (\alpha_a(\mu_a)_j + (1 - \alpha_a)(\mu_b)_j)\right) \cdot \left((\mu_a)_k - (\alpha_a(\mu_a)_k + (1 - \alpha_a)(\mu_b)_k)\right) \\ &\quad + (1 - \alpha_a)\left((\mu_b)_j - (\alpha_a(\mu_a)_j + (1 - \alpha_a)(\mu_b)_j)\right) \cdot \left((\mu_b)_k - (\alpha_a(\mu_a)_k + (1 - \alpha_a)(\mu_b)_k)\right) \\ &= \alpha_a(\Sigma_a)_{jk} + (1 - \alpha_a)(\Sigma_b)_{jk} \\ &\quad + \alpha_a\left((\mu_a)_j - (\alpha_a(\mu_a)_j + (1 - \alpha_a)(-\mu_a)_j)\right) \cdot \left((\mu_a)_k - (\alpha_a(\mu_a)_k + (1 - \alpha_a)(-\mu_a)_k)\right) \\ &\quad + (1 - \alpha_a)\left((-\mu_a)_j - (\alpha_a(\mu_a)_j + (1 - \alpha_a)(-\mu_a)_j)\right) \cdot \left((-\mu_a)_k - (\alpha_a(\mu_a)_k + (1 - \alpha_a)(-\mu_a)_k)\right) \end{aligned} \quad (16)$$

Putting it all together, we arrive at the following decomposition of the synthetic data distribution covariance matrix:

$$(\Sigma) = \alpha_a(\Sigma_a) + (1 - \alpha_a)(\Sigma_b) + 4\alpha_a(1 - \alpha_a)\mu_a\mu_a^\top \quad (18)$$

A.3 Adversarial Attacks

To solve the optimization problem posed in eq. (10), we examine the likelihood function. Let $p_{\mathcal{D}_g}$ now denote the PDF of the image of distribution \mathcal{D}_g as it appears in the 1-D PCA embedding space. We assume $\gamma \leq 1$. We aim to find the strength of the perturbation necessary to push an example \mathbf{x} in a $\frac{p_{\mathcal{D}_a}[\mathbf{f}(\mathbf{x}+\boldsymbol{\delta})]}{p_{\mathcal{D}_b}[\mathbf{f}(\mathbf{x}+\boldsymbol{\delta})]}$ exceeds one, where:

$$1 \leq \left(\frac{p_{\mathcal{D}_a} \left[\mathbf{f}(\mathbf{x} + \boldsymbol{\delta}) \mid \boldsymbol{\delta} \propto \frac{(\boldsymbol{\mu}_b - \mathbf{x})}{\|\boldsymbol{\mu}_b - \mathbf{x}\|_2} \right]}{p_{\mathcal{D}_b} \left[\mathbf{f}(\mathbf{x} + \boldsymbol{\delta}) \mid \boldsymbol{\delta} \propto \frac{(\boldsymbol{\mu}_b - \mathbf{x})}{\|\boldsymbol{\mu}_b - \mathbf{x}\|_2} \right]} \right) \quad (19)$$

$$= \left((2\pi)^{-1/2} (f(\mathbf{q}_1))^{-1} \right) \cdot \exp \left\{ -\frac{1}{2} \left[\mathbf{f} \left(\mathbf{x} + \eta \frac{(\boldsymbol{\mu}_b - \mathbf{x})}{\|\boldsymbol{\mu}_b - \mathbf{x}\|_2} - \boldsymbol{\mu}_a \right) \right]^2 (f(\mathbf{q}_1))^{-2} \right\} \quad (20)$$

$$\times \left[\left((2\gamma\pi)^{-1/2} (f(\mathbf{q}_1))^{-1} \right) \cdot \exp \left\{ -\frac{\gamma}{2} \cdot \left[\mathbf{f} \left(\mathbf{x} + \eta \frac{(\boldsymbol{\mu}_b - \mathbf{x})}{\|\boldsymbol{\mu}_b - \mathbf{x}\|_2} - \boldsymbol{\mu}_b \right) \right]^2 (f(\mathbf{q}_1))^{-2} \right\} \right]^{-1} \\ \leq \exp \left\{ -\frac{1}{2} \left[\mathbf{f} \left(\mathbf{x} + \eta \frac{(\boldsymbol{\mu}_b - \mathbf{x})}{\|\boldsymbol{\mu}_b - \mathbf{x}\|_2} \right) + f(\boldsymbol{\mu}_b) \right]^2 \right\} \cdot \left[\exp \left\{ -\frac{\gamma}{2} \cdot \left[\mathbf{f} \left(\mathbf{x} + \eta \frac{(\boldsymbol{\mu}_b - \mathbf{x})}{\|\boldsymbol{\mu}_b - \mathbf{x}\|_2} \right) - f(\boldsymbol{\mu}_b) \right]^2 \right\} \right]^{-1} \quad (21)$$

We now solve the following the following inequality for η

$$1 \leq \exp \left\{ -\frac{1}{2} \left[\mathbf{f} \left(\mathbf{x} + \eta \frac{(\boldsymbol{\mu}_b - \mathbf{x})}{\|\boldsymbol{\mu}_b - \mathbf{x}\|_2} \right) + f(\boldsymbol{\mu}_b) \right]^2 \right\} \cdot \left[\exp \left\{ -\frac{\gamma}{2} \cdot \left[\mathbf{f} \left(\mathbf{x} + \eta \frac{(\boldsymbol{\mu}_b - \mathbf{x})}{\|\boldsymbol{\mu}_b - \mathbf{x}\|_2} \right) - f(\boldsymbol{\mu}_b) \right]^2 \right\} \right]^{-1} \quad (22)$$

After some algebra, we arrive at the following interval solution for η .

$$\eta > \frac{2b(1-\gamma)\sqrt{\frac{a^2\gamma}{b^2(\gamma-1)^2} + a\gamma + a + f(\boldsymbol{\mu}_b)(1-\gamma)}}{b(\gamma-1)} \quad (23)$$

AND

$$\eta < \frac{2b(\gamma-1)\sqrt{\frac{a^2\gamma}{b^2(\gamma-1)^2} + a\gamma + a + f(\boldsymbol{\mu}_b)(1-\gamma)}}{b(\gamma-1)} \quad (24)$$

Where, for notational compactness, we denoted the following:

$$a = f(\mathbf{x}) \quad (25)$$

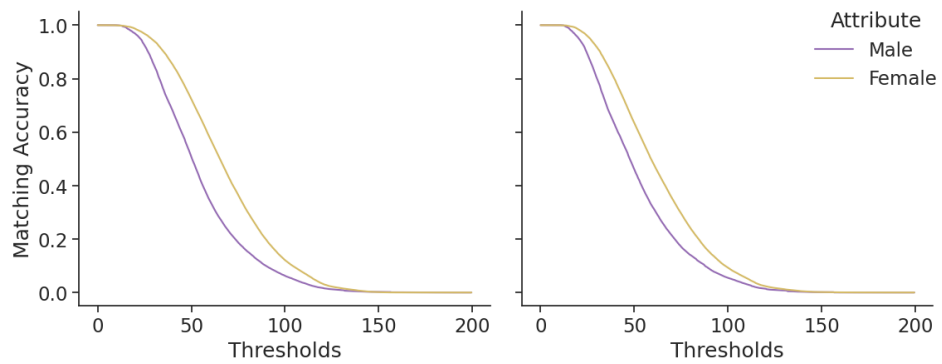
$$b = f \left(\frac{(\boldsymbol{\mu}_b - \mathbf{x})}{\|\boldsymbol{\mu}_b - \mathbf{x}\|_2} \right) \quad (26)$$

Since the right-side of inequality (22) upper bounds the right-side of inequality (19), we know that any solution for inequality (22) is also a solution for inequality (19).

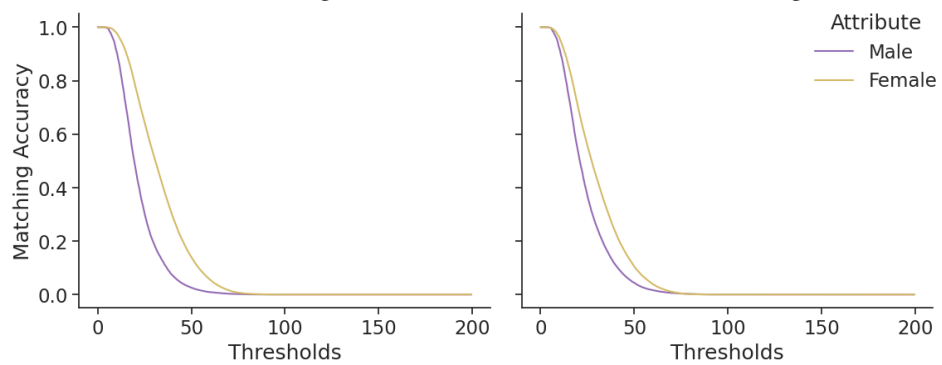
Since inequality (24) is a bound on ϵ which provides a guarantee on when eq. (10) is infeasible. Hence we conclude that eq. (10) may be feasible only when

$$\epsilon \geq \max \left\{ 0, \frac{2b(\gamma-1)\sqrt{\frac{a^2\gamma}{b^2(\gamma-1)^2} + a\gamma + a + f(\boldsymbol{\mu}_b)(1-\gamma)}}{b(\gamma-1)} \right\} \quad (27)$$

B Additional Experiments



(a) Imbalanced, Targeted: Different Race (Left), Same Race (Right)



(b) Balanced, Targeted: Different Sex (Left), Same Sex (Right)

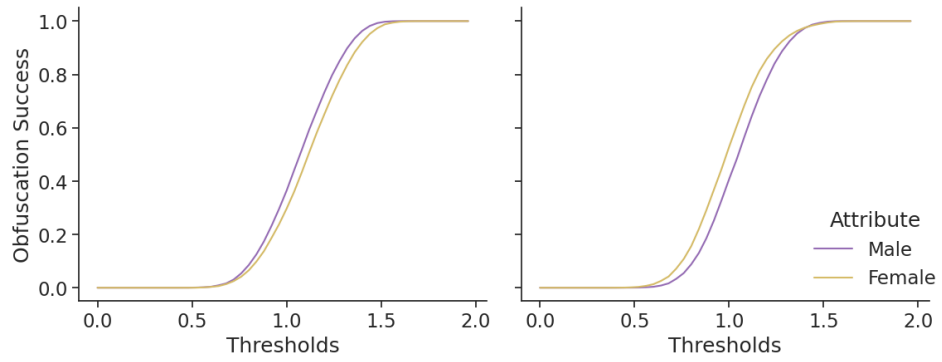
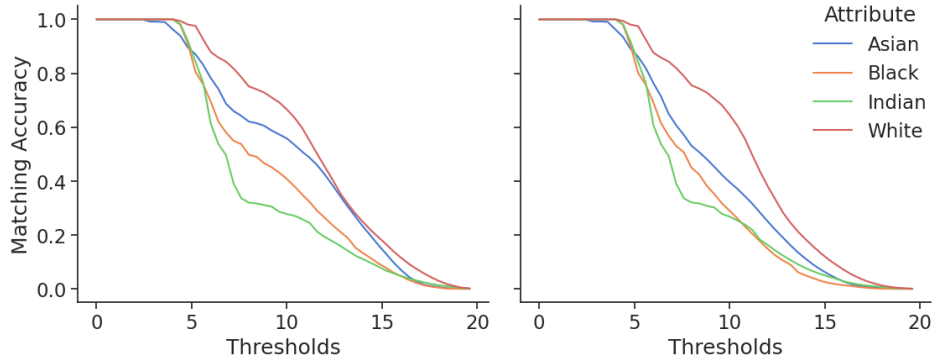
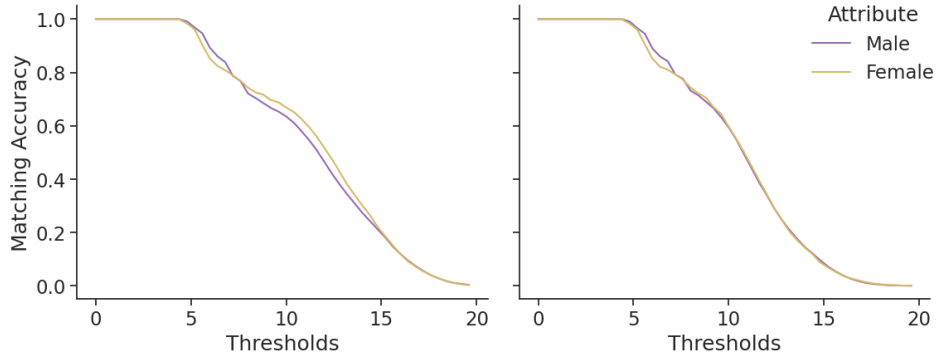


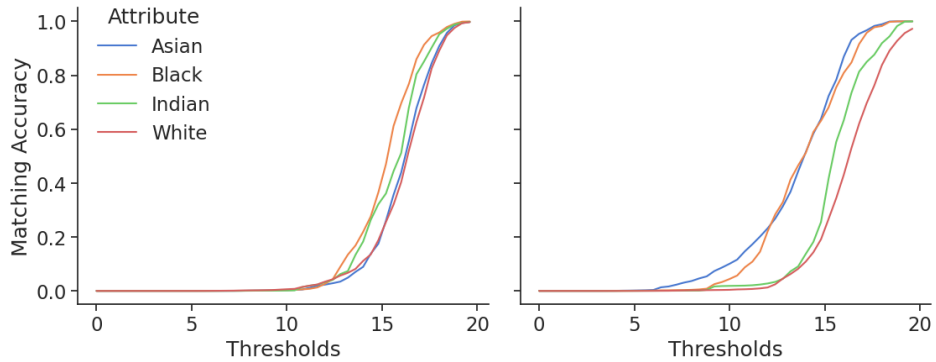
Figure 15: Untargeted obfuscation success on OpenFace in a black-box setting. Generating examples on the balanced model still results in disparities in the target model.



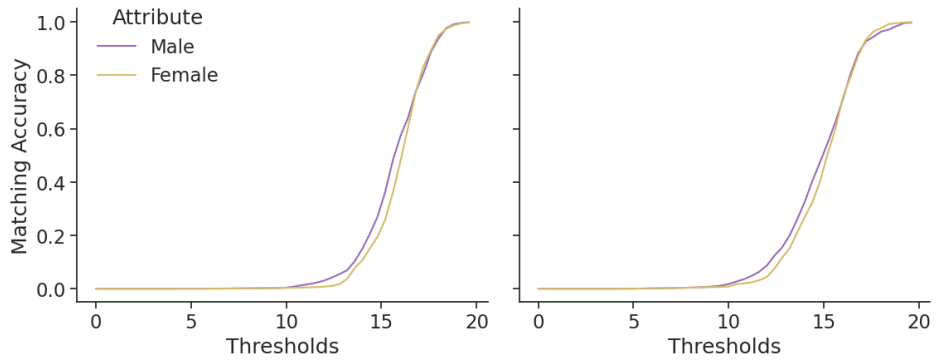
(a) Targeted: Different (Left) vs. Same (Right) Race



(b) Targeted: Different (Left) vs. Same (Right) Sex



(c) Untargeted: Different (Left) vs. Same (Right) Race



(d) Untargeted: Different (Left) vs. Same (Right) Sex

Figure 16: Targeted obfuscation success evaluated on FaceNet in a white-box setting.